Acta Crystallographica Section D
Biological Crystallography
ISSN 0907-4449

Synchrotron white-beam X-ray topography of ribonuclease S crystals

W. M. Vetter,[a]* D. T. Gallagher[b] and M. Dudley[a]

[a]Department of Materials Science and Engineering, State University of New York at Stony Brook, Stony Brook NY 11794-2275, USA, and [b]NIST Biotechnology Division, Gaithersburg, MD 20899-8312, USA

Correspondence e-mail: wvetter@ms.cc.sunysb.edu

Received 4 October 2001
Accepted 21 January 2002

With careful experimental design, indexed synchrotron white-beam X-ray topographs of ribonuclease S crystals at ambient temperature could be recorded with a definition and contrast comparable to that of monochromatic beam topographs of other proteins reported in the literature. By excluding wavelengths longer than 1 Å from the white beam with a filter, a radiation dose equivalent to that required to record about 18 topographs could be tolerated without appreciable radiation damage to the samples. Bragg angles of 0.5° or less were required to select low-index harmonically pure reflections with high intensities and extinction lengths only several times the sample's thickness. The resulting X-ray topographs in some cases showed topographic detail and in others showed the even featureless background that has been considered characteristic of a protein crystal of low mosaicity. The ribonuclease S crystals were well ordered single crystals of a quality comparable to other protein crystals that have been studied by X-ray topography.

1. Introduction

Clinical medicine, biological science and nanotechnology share a demand for detailed information concerning the molecular structures of proteins. Because X-ray diffraction is the most successful method of measuring them, progress often depends on being able to grow crystals of specific proteins with suitable diffracting strength. Unfortunately, macromolecular crystal growth is difficult to understand and control, so that obtaining adequate crystals remains a bottleneck in the determination of protein structures at desired resolutions. Means are required to analyze the solid-state character of the crystals being produced by the varied growth methods being brought to bear on this problem.

By providing images of internal features responsible for local variations in diffraction intensity, X-ray topography enables detailed analyses of crystal quality. A number of X-ray topographic studies of protein crystals have appeared in the literature, mainly applied to crystals of tetragonal lysozyme (Izumi *et al.*, 1996; Stojanoff & Siddons, 1996; Stojanoff *et al.*, 1997; Dobrianov *et al.*, 1998, 1999; Caylor *et al.*, 1999; Fourme *et al.*, 1999; Otalora *et al.*, 1999; Vidal *et al.*, 1999; Boggon *et al.*, 2000; Hu *et al.*, 2001). These studies have yielded information on protein crystal growth, particularly on the relation between growth conditions and defects. As the sensitivity and resolution of detectors used in diffractometry continues to improve and a wider variety of proteins and growth conditions are examined, the use of X-ray topography as a tool for the analysis of protein crystal quality increases in importance.

Protein crystals tend to suffer severe and rapid degradation from the intensity of a white (polychromatic) synchrotron beam. Possibly this is a reason why monochromatic X-rays have been used for topography in all of the above-cited studies except one (Izumi *et al.*, 1996). Still, white synchrotron radiation is sometimes tolerated long enough to enable time-resolved structural studies (Moffat, 2001).

By its nature, synchrotron white-beam X-ray topography demands no specialized beam conditioning or peak-detection apparatus; it requires a sheet of X-ray film enclosed in a cassette. In cases where a crystal's lattice is bent, white-beam topography will give topographs that represent the entire projected volume of a crystal, whereas a topograph obtained with a monochromatic beam images the area of the crystal that lies within the crystal's diffracting range for that monochromatic beam, representing contours of orientation only. Another advantage is that the white-beam method simultaneously produces many images of the crystal in a single exposure, whereas techniques using monochromatic radiation can only produce one at a time. As synchrotron white-beam topography is then desirable in certain research situations, the evaluation of diffraction behavior and the useful lifetime of proteins under white-beam conditions are important preludes to their topographic study.

Ribonuclease S (RNase S) was one of the first protein structures to be determined by diffraction (Wyckoff *et al.*, 1970) and its crystal forms are well characterized (Kim *et al.*, 1992). It is derived from ribonuclease A by subtilisin (protease) treatment, which breaks one specific peptide bond (between residues 20 and 21), cleaving the 124-residue polypeptide into two chains; the chains remain associated and the enzyme remains active. Three crystal forms have been reported for RNase S (Mitsui & Wyckoff, 1975). The trigonal crystal form is well suited to the present study: the crystals grow reproducibly with nearly isometric shape to ~0.4 mm in size and, for protein crystals, they have relatively high quality and low mosaicity. In this study, the optimum conditions for the white-beam topography of RNase S crystals, the typical characteristics of topographs taken under these conditions and the crystals' useful lifetime in the beam were determined.

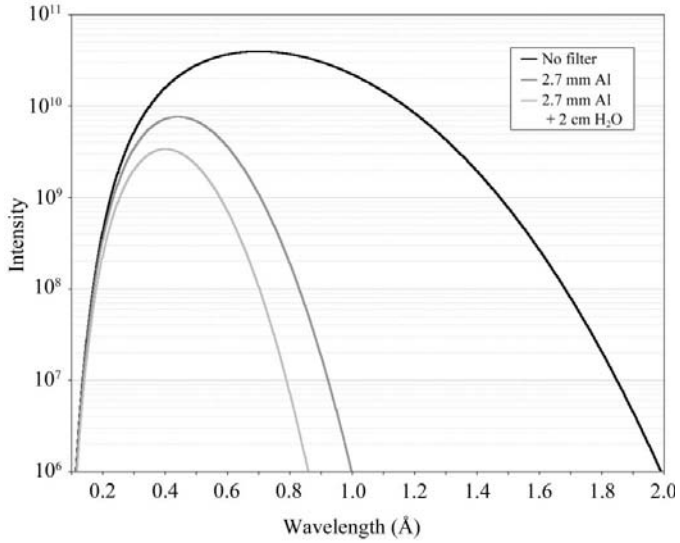

Figure 1
White-beam profiles obtained at beamline X19-C. The effect on the white-beam spectrum (generated using the storage ring's 2.801 GeV mode) of filtration through an aluminium plate and through a 2.7 mm aluminium plate plus 20.0 mm of water is shown. The intensity scale is logarithmic. Its units are photons per 10^{-3} Å bandwidth per mA of ring current per mrad of ring acceptance angle per mrad of vertical beam divergence per second.

2. Experimental procedure

Bovine RNase S was purchased from Sigma and crystallized (space group $P3_121$; unit-cell parameters a = 44.5, c = 97.3 Å) at pH 5.0 from 100 m*M* sodium acetate, 0.9 *M* ammonium sulfate, 3.0 *M* NaCl in a DCCS crystal-growth device developed by BioSpace International (DBA BSI Proteomics, Gaithersburg, MD 20877, USA) as described in Gallagher *et al.* (2002). Crystals of 0.3–0.4 mm width were sealed in glass capillaries together with a few microlitres of mother liquor trapped at one end; the crystals adhered to the capillary walls by a film of mother liquor. These capillaries were mounted on the goniometer at the Stony Brook Synchrotron Topography Station, beamline X-19C, at the National Synchrotron Light Source at Brookhaven National Laboratory.

Several attenuation strategies were tested to reduce the intensity of the raw white beam of 1 mm^2 cross section. Most of the topographic exposures utilized a 2.7 mm thick plate of aluminium as a filter, either alone or in conjunction with two 1.0 cm plastic cuvettes filled with water. For crystal alignment, Laue patterns were recorded in 15 s exposures on 13 × 18 cm sheets of medical X-ray film placed perpendicular to the incident beam at a specimen-to-film distance of 20 cm. After alignment, topographs were recorded on 20.5 × 25.4 cm sheets of Kodak Industrex SR-1 film in exposures of 180 s or shorter. The films were protected from radiation scattered from the incident beam's passage through air by a lead plate with a 4 mm wide hole mounted 10 cm upstream from the sample. Low Bragg angles (~0.5°) required a square of lead as small as 3 mm wide to be taped to the film cassette as a beam stop.

Calculations of incident synchrotron beam photon flux at 0.001 Å spectral bandwidth were performed using a Microsoft *Excel* spreadsheet. For these calculations, the wavelength range of the white beam, 0.100–2.000 Å, was divided into 0.001 Å segments. Flux values for each segment across the beamline spectrum were summed to obtain values for the total photon flux. For each segment, the dose absorbed by the RNase S crystals was determined from each segment's linear absorption coefficient as calculated from the protein's molecular formula and the crystals' known solvent fraction of 38% water. The dose absorbed for each segment was then summed to obtain the total dose.

3. Results and discussion

The RNase S crystals decomposed in X19-C's unfiltered white beam during a single exposure of less than 10 s owing to

radiation damage. It is unlikely that heating of the crystal by the white beam caused this decomposition, since we have calculated the adiabatic temperature rise for a crystal under the unfiltered incident beam intensity using a formula given by Helliwell (1984) to be 0.14 K s^{-1}, which indicated the samples were warmed by only a few kelvin during an exposure. Filtration of the raw beam through a 2.7 mm thick aluminium plate was calculated to reduce the total intensity by an order of magnitude and to shift the wavelength of the maximum intensity from 0.8 to 0.5 Å. This effect is shown graphically in Fig. 1. This filtration removed most of the intensity above 1 Å. While similar white-beam filtration experiments conducted on cryocooled lysozyme crystals (cryocooling protein crystals is widely used to extend their lifetimes in synchrotron diffractometry) showed no effect on the dose absorbed during their decomposition (Gonzalez & Nave, 1994), at ambient temperatures long-wavelength radiation is recognized as being significantly more destructive to proteins than shorter wavelengths (Arndt, 1984). With the Al filter, the rapid deterioration of the crystal that occurred in the unfiltered beam was not observed.

Diffraction spots recorded on X-ray film were generally faint compared with background noise; therefore, steps were taken to reduce radiation scattered by the synchrotron beam's passage through the air in the beamline hutch and by its collision with the crystal's glass capillary mount. Decreasing the cross-sectional area of the filtered incident beam until it bracketed the crystal minimized the source of the incoherent scatter. The film was protected from radiation scattered by air by directing the incident beam through a small hole in a lead plate upstream from the sample. Choosing a specimen-to-film distance of 20 cm spreads the spots adequately from one another and the transmitted beam and reduces the area density of the background noise resulting from diffuse scatter from the crystal and its capillary as much as possible before the theoretical maximum topographic resolution is diminished.

Under these conditions, images comparable to published monochromatic beam topographs could be obtained with an exposure in the range of 2.5 min. A crystal could be aligned to the $(11\bar{2}0)$ face by visual inspection of its morphology, followed by analysis of Laue patterns recorded on medical X-ray film (blue sensitive). Because medical film records this filtered beam spectrum about eight times faster than industrial film, it was possible to obtain a suitable Laue pattern in 15 s and to align the crystal in less than 4 min of total exposure (exposing about ten medical films). The filtration served to reduce the number of spots and the complexity of the Laue pattern so that low-index reflections could be more easily identified. As the crystal is rotated a few degrees from alignment to the $[1\bar{2}10]$ zone axis (a $\{11\bar{2}0\}$ plane normal), low-index diffraction spots of the $[1\bar{2}10]$ zone appear arranged in an elliptical pattern, which are straightforward to index in the otherwise complex protein Laue pattern. The most important of these reflections for X-ray topography, among which are those with the largest structure factors in the crystal, are $10\bar{1}1$, $10\bar{1}3$, $10\bar{1}0$ and 0003.

Fig. 2 shows topographs of an RNase S crystal taken over a period of 2 h exposure in a beam filtered through 2.7 mm of aluminium and then through two 1.0 cm plastic cuvettes filled with water. The detail in the image represents the precipitate trapped in the crystal which was visible under a microscope. The images remain well defined and show internal detail during the first hour. After 40 min the detail begins to noticeably degrade and after 60 min the outline of the crystal grows diffuse. Over the next hour the diffraction spots eventually vanished. At that point, the physical shape of the crystal was unchanged, but it had yellowed. The additional filtration through 20 mm water decreases the beam intensity and extends a crystal's lifetime in the beam further, but offered little advantage, as has been suggested by Izumi *et al.* (1996), over an increased thickness of aluminium. The effect of filtration through water on the beam profile is shown in Fig. 1. Because the linear absorption coefficient of water plotted against X-ray wavelength has a smaller curvature compared with that of aluminium, water tends to decrease the total intensity of the beam as opposed to preferentially excluding long-wavelength radiation. It should be noted that the linear absorption curves of neither material contain an absorption edge that might sharply exclude a wavelength that the other transmits. Decomposition experiments similar to that depicted in Fig. 2 were carried out without a filter of water, using 2.7 mm aluminium only, although the particular crystals used lacked the interesting topographic contrast visible in Fig. 2. These experiments gave similar results, but the image degraded over a timescale proportionally shorter to the intensity of the incident beam.

Numerically, the white beam X-ray intensity (at a synchrotron storage ring current of 250 mA) incident on a crystal 0.3 mm wide is 8.9×10^{11} photons s^{-1} (1.8×10^{14} keV mm^{-2} s^{-1}), for the white beam filtered through 2.7 mm Al it is 8.2×10^{10} photons s^{-1} (2.6×10^{13} keV mm^{-2} s^{-1}) and after filtration through 2.7 mm Al

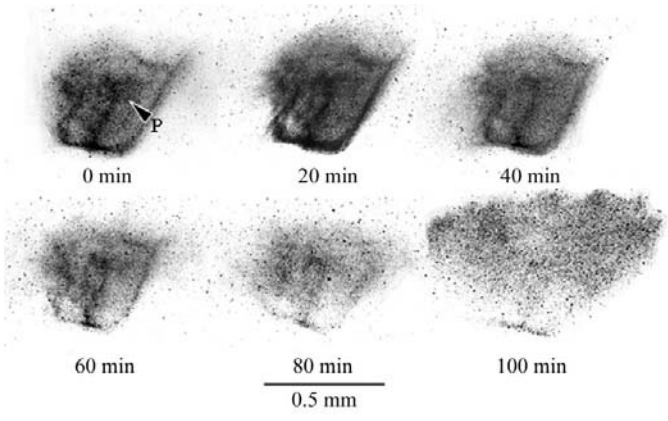

Figure 2
Decomposition of an RNase S crystal in the filtered white beam. Series of filtered white-beam X-ray topographs ($\mathbf{g} = 20\bar{2}8$, $\lambda = 0.47$ Å) of an RNase S crystal illustrating the progress of its decomposition in the beam. Dark contrast arising from precipitate included in the crystal is indicated by P. The total photon flux incident on the crystal is about 5.2×10^{12} photons min^{-1} mm^{-2}; the absorbed dose is about 12 Gy min^{-1}.

and 20.0 mm H_2O is 3.1×10^{10} photons s^{-1} (1.1×10^{13} keV mm^{-2} s^{-1}). For comparison, a 1.6 kW Cu $K\alpha$ rotating-anode source, which might be used for protein diffractometry, delivers, through a 15 cm collimator, about 6.4×10^7 photons s^{-1} (Harmsen *et al.*, 1976). The dose absorbed by a 0.3 mm thick RNase S crystal during 15 s in the unfiltered white beam is 53 Gy; using a beam filtered through 2.7 mm Al, a 15 s exposure for alignment delivers 7.5 Gy and a 2.5 min exposure for topography delivers a 75 Gy dose. The increase in crystal lifetime with the filtration then results from the elimination of long-wavelength radiation rather than any decrease in total dose during a topographic experiment. The point at which the image of the RNase S crystal shown in Fig. 2 began to degrade (40 min) corresponds to a dose of about 1.2 kGy; afterwards the intensity of the image progressively diminished, while the outline of the topograph remained unchanged and its internal detail remained visible for the next 1.8 kGy (until 60 min). Further exposure diffused the image's outline, degraded the contrast of its internal detail and eventually stretched the image into an asterism. After 3.6 kGy of irradiation, all spots in the crystal's Laue pattern vanished. It is interesting to compare these values with the experiments of Gonzalez *et al.* (1992), which were carried out at 100 K where secondary decomposition mechanisms are suppressed, in which doses on the order of 1 GGy were required to decompose lysozyme crystals in a synchrotron white beam.

White-beam topographic reflections of crystals with large lattice constants have a greater tendency to suffer from harmonic contamination (Vetter & Dudley, 1998). As a crystal is turned, the Bragg angles of its reflections change and so do their diffracting wavelengths. The broader the white-beam spectrum, the more harmonics that may simultaneously satisfy Bragg's law contribute to the topograph. The relative contributions of the series of harmonic reflections were calculated using beam profile intensities and theoretical relationships derived for perfect crystals. The relative diffracted intensities contributed by the harmonics were obtained using the equation (Hart, 1975)

$$I_h = P(\lambda)F_{hkl}\lambda^3 \mathrm{cosec}^2\theta, \quad (1)$$

where $P(\lambda)$ is the distribution of X-ray intensity with wavelength λ at beamline X19-C arriving at the sample after filtration through 2.7 mm aluminium (shown graphically in Fig. 1), F_{hkl} is the reflection's structure factor and θ is the Bragg angle. Values of I_h, after considering atmospheric attenuation between the specimen and film, were used to calculate the proportions of film grains rendered developable (Brown *et al.*, 1976). The relative proportions of film grains rendered developable by exposure to each harmonic wavelength determine the contribution of each harmonic. The relative contributions of harmonic intensity for harmonics of the reflection $10\bar{1}1$ *versus* Bragg angle are shown in Fig. 3. It can be seen that when the Bragg angle is below 0.5° the topograph is mainly of $10\bar{1}1$. Above about 0.5° this reflection becomes severely contaminated, consisting of three or more harmonics. At a Bragg angle of 0.50° the $10\bar{1}1$ reflection suffers 3% harmonic contamination (by $20\bar{2}2$), which is acceptable, as it is unlikely to degrade image detail or contrast. Other low-index reflections behave similarly, suffering little harmonic contamination below Bragg angles of 0.5°.

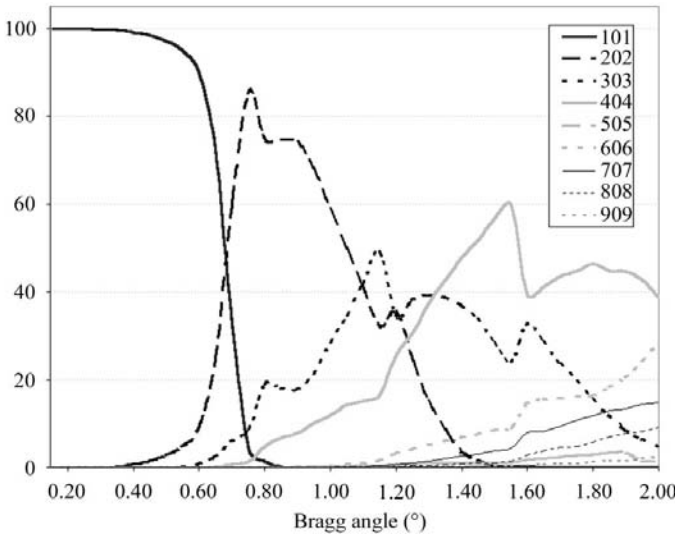

Figure 3
Harmonic composition of $n(10\bar{1}1)$ topographs across a range of Bragg angle. Each line represents the individual contribution of a harmonic of $10\bar{1}1$. Sudden drops and rises in a harmonic's intensity are associated with the K absorption edge of silver (the X-ray film's sensitivity is based on grains of silver bromide).

To record topographs at these low angles, the longest useful specimen-to-film distance (20 cm), the narrowest possible incident beam and the smallest possible incident beam stop (a 3 mm square of 0.8 mm lead sheet) were required to minimize background noise. When θ is less than 0.5°, low-index reflections become more intense and topographs may be recorded on industrial X-ray film with an exposure to the filtered beam of 100 s or less. In this way, the sharpest most contrast-rich topographs could be obtained. Some of these are shown in Fig. 4. Note that for semiconductors or ionic salts, optimum Bragg angles for X-ray topography typically lie between 5 and 12°.

When a reflection is properly indexed, its most intense harmonic is identified and its Bragg angle is known, the diffraction wavelength can be calculated. The diffraction wavelength is normally reported with the publication of an X-ray topograph for the sake of scientific reproducibility. At a Bragg angle of 0.50° this wavelength for the $10\bar{1}1$ reflection is 0.63 Å. It should be noted that as these crystals are mounted against the wall of a capillary by a film of their mother liquor, in a minority of cases they may shift by several degrees into a new orientation during the length of exposure required for industrial film (the incident beam intensity is not high enough to thermally decay the crystal, but it seems to warm the crystal enough to sometimes make it move). In these cases, it can be possible to index a spot, but it is impossible to *choose* a desired Bragg angle.

Fig. 4 shows the quality of topographs that may be obtained with this level of orientation control. They show some of the characteristics that have been reported in the literature for

lysozyme crystals: a featureless bulk in the case of Figs. 4(*a*) and 4(*c*) (Dobrianov *et al.*, 1998) and sectorial contrast in Fig. 4(*b*) (Vidal *et al.*, 1999). Images of included precipitates, as seen in the topographs in Fig. 2, have also been reported for lysozyme (Stojanoff *et al.*, 1997). Among the features from the literature of lysozyme that were not observed in these crystals were gross asterism and misorientation across subgrain boundaries (Izumi *et al.*, 1996) and the presence of a macromosaic structure whose individual mosaic blocks are resolvable by X-ray topography (Hu *et al.*, 2001). In a few of the RNase S crystals, as in Fig. 4(*d*), an unusual crystal with one rounded side and few well developed facets, dark contrast surrounded the point of crystal nucleation, indicating the presence of strain in that part of crystal formed during early stages of growth. While the quality of the crystals varied somewhat, all showed an outline faithful to the crystal's shape, possibly including the shadow of an edge between two crystal facets, but otherwise with little topographic detail. A uniform topograph, free of dark contrast indicating stress, is usually considered indicative of a protein crystal with a low mosaicity.

The dynamical extinction length for a symmetrical reflection in a perfect crystal is

$$\xi_g = (\pi/r_e)V_C \cos\theta/F_{hkl}\lambda, \qquad (2)$$

where r_e is the classical electron radius and V_C is the unit-cell volume. The dominant factor determining the extinction length of a given reflection in a protein crystal is the ratio of the cell volume to its structure factor. Otalora *et al.* (1999) have pointed out that the extinction lengths for crystallographic reflections of proteins commonly studied are much larger than those for crystals of small molecules and are sometimes as much as an order of magnitude longer than the dimensions of the protein crystals available. They noted that though still great, the extinction lengths for lysozyme, if the uncertainty in calculated values of protein structure factors is considered, may indicate that diffraction in lysozyme lies within the regimes of either kinematical or dynamical theories. Generally, at the point when a crystal's thickness is less than one quarter of a reflection's extinction length, images of dislocations in X-ray topographs are absent (Tanner, 1972). Some researchers point out features in lysozyme topographs that might be regarded as dislocations and Dobrianov *et al.* (1998, 1999) have published topographs of crystals which underwent abrupt changes in growth conditions in which lines of dark contrast radiate outward along the growth direction. No dislocation lines were visible in our topographs of RNase S. For this observation to have meaning, the sensitivity of these topographs toward defect contrast must be taken into consideration.

For $10\bar{1}1$, the reflection with the largest structure factor in the crystal (6025.0), at a Bragg angle of 0.50°, the extinction length is 0.78 mm. At this Bragg angle, $10\bar{1}1$ is 3% harmonically contaminated by its first harmonic, $20\bar{2}2$, which has an extinction length of 13 mm. If the Bragg angle is increased to 0.75°, at which angle $20\bar{2}2$ reaches its highest harmonic purity, 85% (this may be seen in Fig. 3), the extinction length of $20\bar{2}2$ is 8.8 mm. Calculated values for the extinction lengths of the reflections with the five largest structure factors in the crystal are a few multiples of the thickness of a RNase S crystal at low Bragg angles. The Bragg angle may be increased to reduce the extinction length further, but this is at the cost of contaminating the reflection with harmonics that have extinction lengths that are orders of magnitude longer than the crystal's dimensions. To obtain meaningful topographs using the white-beam method, it is therefore important to control the crystal's orientation, to index and choose diffraction spots carefully and select favorable Bragg angles.

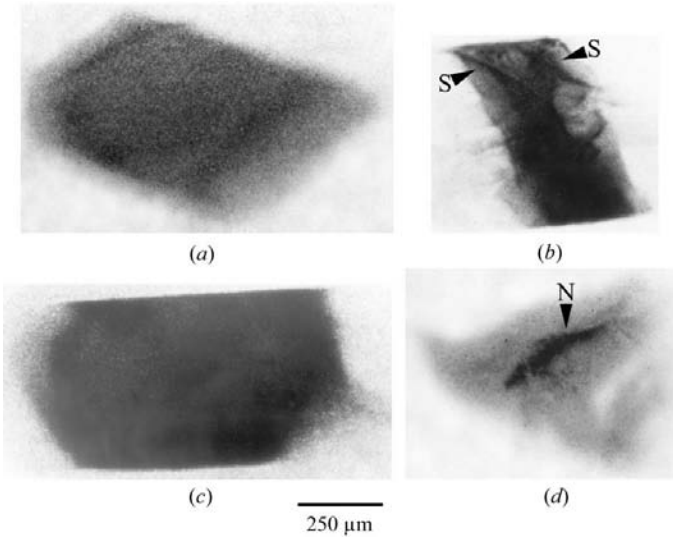

Figure 4
Synchrotron white-beam X-ray topographs of RNase S crystals. $\mathbf{g} = 10\bar{1}1$, $\lambda = 0.63$ Å. Dark contrast in (*b*) that may be associated with growth sectors is indicated by S and central dark contrast in (*d*) at the point of crystal nucleation is indicated by N. The photographic grain is visible in these topographs, which is normal at this level of magnification, and tends to be emphasized when the background noise level is significant.

4. Conclusions

With appropriate filtration of the white beam, careful attention to background-noise reduction and crystal alignment using fast film, indexed synchrotron white-beam topographs of protein crystals could be recorded with a definition and contrast equal to that of monochromatic beam topographs reported in the literature. This could be accomplished without damaging the samples appreciably during the experiment. Small Bragg angles were required to select low-index harmonically pure reflections desirable for their shorter extinction lengths, which place their diffraction within the realm of dynamical theory. Topographs taken under these conditions sometimes showed features that could be considered as dynamical contrast, but more often displayed a featureless bulk of low diffracting intensity. The resulting X-ray topographs showed that the RNase S crystals were well defined single crystals of a quality comparable to that of hen egg-white lysozyme crystals, which other researchers have evaluated using X-ray topography.

The authors are grateful to David Black for helpful discussions and to Carrie Stover and David Charlton for assistance in crystal cultivation. Topography was carried out at the Stony Brook Synchrotron Topography Facility, beamline X19-C, at the NSLS, which is supported by the US Department of Energy. Certain commercial equipment, software and materials are identified in this paper to specify the experimental procedure. In no case does such identification imply recommendation or endorsement by the National Institute of Standards and Technology, nor does it imply that the material or equipment is necessarily the best available for the purpose.

References

Arndt, U. W. (1984). *J. Appl. Cryst.* **17**, 118–119.
Boggon, T. J., Helliwell, J. R., Judge, R. A., Olczak, A., Siddons, D. P., Snell, E. H. & Stojanoff, V. (2000). *Acta Cryst.* D**56**, 868–880.
Brown, D. B., Criss, J. W. & Birks, L. S. (1976). *J. Appl. Phys.* **47**, 3722–3731.
Caylor, C. L., Dobrianov, I., Lemay, S. G., Kimmer, C., Kriminski, S., Finkelstein, K. D., Zipfel, W., Webb, W. W., Thomas, B. R., Chernov, A. A. & Thorne, R. E. (1999). *Proteins*, **36**, 270–281.
Dobrianov, I., Finkelstein, K. D., Lemay, S. G. & Thorne, R. E. (1998). *Acta Cryst.* D**54**, 922–937.
Dobrianov, I., Finkelstein, K. D., Lemay, S. G. & Thorne, R. E. (1999). *J. Cryst. Growth*, **196**, 511–523.
Fourme, R., Ducruix, A., Riès-Kautt, M. & Capelle, B. (1999). *J. Cryst. Growth*, **196**, 535–545.
Gallagher, T., Stover, C., Moses, J., Charlton, D., Steinberg, E. & Arnowitz, L. (2002). Submitted.
Gonzalez, A. & Nave, C. (1994). *Acta Cryst.* D**50**, 874–877.
Gonzalez, A., Thompson, A. W. & Nave, C. (1992). *Rev. Sci. Instrum.* **63**, 1177–1180.
Harmsen, A., Leberman, R. & Schulz, G. E. (1976). *J. Mol. Biol.* **104**, 311–314.
Hart, M. (1975). *J. Appl. Cryst.* **8**, 436–444.
Helliwell, J. R. (1984). *Rep. Prog. Phys.* **47**, 1403–1497.
Hu, Z. W., Thomas, B. R. & Chernov, A. A. (2001). *Acta Cryst.* D**57**, 840–846.
Izumi, K., Sawamura, S. & Ataka, M. (1996). *J. Cryst. Growth*, **168**, 106–111.
Kim, E. E., Varadarajan, R., Wyckoff, H. W. & Richards, F. M. (1992). *Biochemistry*, **31**, 12304–12314.
Mitsui, Y. & Wyckoff, H. W. (1975). *J. Mol. Biol.* **94**, 17–31.
Moffat, K. (2001). *Chem. Rev.* **101**, 1569–1581.
Otalora, F., Garcia-Ruiz, J. M., Gavira, J. A. & Capelle, B. (1999). *J. Cryst. Growth*, **196**, 546–558.
Stojanoff, V. & Siddons, D. P. (1996). *Acta Cryst.* A**52**, 498–499.
Stojanoff, V., Siddons, D. P., Monaco, L. A., Vekilov, P. & Rosenberger, F. (1997). *Acta Cryst.* D**53**, 588–595.
Tanner, B. K. (1972). *Phys. Status Solidi A*, **10**, 381–386.
Vetter, W. M. & Dudley, M. (1998). *J. Appl. Cryst.* **31**, 820–822.
Vidal, O., Robert, M. C., Arnoux, B. & Capelle, B. (1999). *J. Cryst. Growth*, **196**, 559–571.
Wyckoff, H. W., Tsernoglou, D., Hanson, A. W., Knox, J. R., Lee, B. & Richards, F. M. (1970). *J. Biol. Chem.* **245**, 305–328.